Experimental Mechanics manuscript No.
(will be inserted by the editor)

Experimental Determination of Lamb Wave Dispersion Diagrams Using 2D Fourier Transform and Laser Vibrometry

Tilmann Barth · Natalie Rauter · Rolf Lammering

Received: date / Accepted: date

T. Barth
Helmut-Schmidt-University/
University of the Federal Armed Forces
Holstenhofweg 85,
22043 Hamburg, Germany
Tel.: +49-40-6541-2745
Fax: +49-40-6541-2034
E-mail: barth@hsu-hh.de
ORCiD: 0000-0002-0667-0609

N. Rauter
Helmut-Schmidt-University/
University of the Federal Armed Forces
Holstenhofweg 85,
22043 Hamburg, Germany
ORCiD: 0000-0003-1704-1426

R. Lammering
Helmut-Schmidt-University/
University of the Federal Armed Forces
Holstenhofweg 85,
22043 Hamburg, Germany
ORCiD: 0000-0002-0867-1859

Abstract

Background: Non-destructive structural health evaluation of thin-walled components on the basis of Lamb wave propagation is a widely used approach. However, most current methods to measure the dispersive behavior of Lamb waves are time based approaches and are not easily capable of high automation to measure influences on the wave propagation along a wide range of frequencies. **Objective:** Develop and validate a highly automatable method to measure Lamb wave dispersion diagrams with high accuracy. To be able to broadband examinate influences, which have only a small effect on the wave propagation. **Methods:** The use of frequency based approaches like the 2d Fourier transform is a known method to measure Lamb waves. This investigation tries to bring together the advantage of the high automation as well as the high accuracy this method offers, by taking into account a non-uniform distribution of the measurement points and using particularly suitable excitation signals for high accuracy. **Results:** The here stated method is capable of automatically creating dispersion diagrams for Lamb waves with high accuracy, automation and reproducibility. The experimental results are compared with analytical results and are in good agreement. **Conclusions:** This investigation shows 2d Fourier transform as a method to create dispersion diagrams of Lamb waves is an accurate and especially highly automatable approach with high accuracy.

Keywords Lamb waves · dispersion curves · 2d Fourier transform · laser vibrometry

1 Introduction

The use of Lamb waves to monitor thin-walled components is a well-known approach in today's Structural Health Monitoring (SHM) [6, 11, 16]. Previous research and applications show that Lamb waves are well suited for this application, but the presence of multimodal waves and their dispersive behavior lead to complex descriptions and elaborate measurements [1, 7, 10, 15, 16, 20, 22]. The multimodal behavior is characterized by the fact that at any given frequency at least two wave modes coexist and a corresponding number of wave packets is contained in sensor signals. The dispersive property of the waves leads to a frequency-dependent phase velocity [6, 7].

The generation of Lamb waves by a piezoelectric wafer and their propagation in an aluminum plate are illustrated in Fig. 1. The measurements are performed with a full-field laser vibrometer, see [11, 13]. The red and green circles represent the out-of-plane velocities of the material points on the surface and the intensity of the color is a measure of the velocity amplitude. Fig. 1 (a) shows the velocity field immediately after wave excitation by a sinusoidal burst signal on the piezoelectric wafer. Fig. 1 (b) shows the propagating Lamb waves at a later time. Here, two wave modes become visible, the symmetric S_0 mode on the outside and the antisymmetric A_0 mode in the interior, indicating the multimodal behavior mentioned above. It is also clear that the symmetric A_0 wave propagates more slowly than the antisymmetric S_0 wave, so that both wave packets separate in the observation period from the left to the right figure due to different velocities. The right figure further shows that the wavelength of the S_0 wave is larger than that of the A_0 wave.

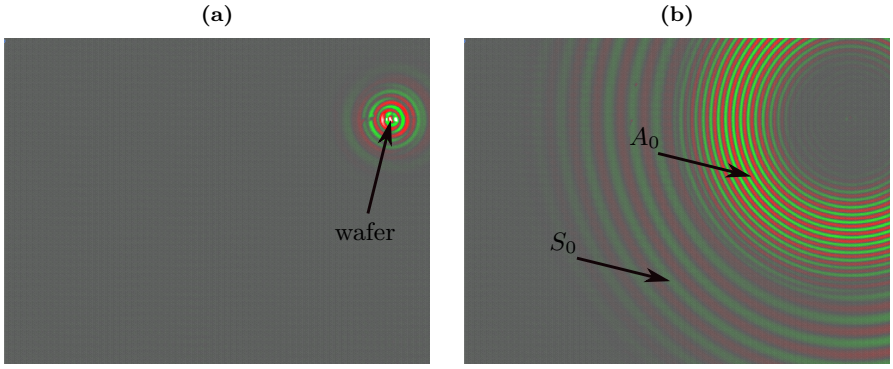

Fig. 1: Symmetric and antisymmetric Lamb waves propagating in an aluminum plate after excitation by a piezoelectric waver. Velocity field immediately after excitation (left) and during further progressing wave propagation (right).

It becomes evident that appropriate methods are needed to capture and assess multimodal behavior. Both time-based and frequency-based methods are available. Considering the occurrence of multiple modes, the use of a frequency-based approach is advantageous over a time-based approach, since the latter can only insufficiently separate the modes if they overlap locally at a certain point in time. With frequency-based approaches, on the other hand, these problems do not arise [5, 23].

Several frequency-based methods can be found in the literature e.g. [2, 8, 9, 14, 15, 18, 21]. Lamb waves exhibit harmonic behavior in both the time and spatial domains, so it is advantageous to apply methods that exploit this property. A frequency-based approach that can be considered for this reason is the two-dimensional Fourier transform (2d-FT) [2, 9, 21]. This method not only provides accurate results, but also allows for a high degree of automation. Therefore, the propagation behavior can be determined over a wide frequency range with minimum effort.

Unlike most other publications that use 2d-FT to evaluate measurements of Lamb waves, the method used here is designed to increase the accuracy of this measurement as much as possible in order to detect even very small deviations resulting from external influences. For these purposes, a multifrequency excitation signal, which is to be considered long in time for this context, and an automated peak search algorithm are used. With these adaptations, the results presented here show that this method is capable of producing whole spectra of dispersion diagrams fully automatically and with high accuracy.

The remainder of this presentation is structured as follows: In Sect. 2 a short review of the theoretical background is given before in Sect. 3 the experimental procedure is described. Sect. 4 then presents the measurement results and evaluates them on the basis of comparisons with analytical data and with respect to their reproducibility. In Sect. 5 a short summary is given and an outlook on future work is presented.

2 Background

2.1 Lamb Waves in Isotropic Solids

The starting point for the analytical solution is the momentum balance for isotropic solids, with neglect of damping. By assuming a linear elastic constitutive law, the stresses are eliminated and the Lamé-Navier differential equation [7] is obtained as

$$(\lambda + \mu)\,\mathrm{grad}\,(\mathrm{div}\ \mathbf{u}) + \mu\ \mathrm{div}\,(\mathrm{grad}\ \mathbf{u}) + \rho\mathbf{b} = \rho\ \frac{\partial^2 \mathbf{u}}{\partial t^2} \tag{1}$$

in which the displacement field $\mathbf{u} = (u_1, u_2, u_3)^T$ serves as independent variable. Moreover, λ and μ are the Lamé constants, ρ is the density, $\mathbf{b}$ the body force density and t denotes the time. For the solution of this differential equation, boundary conditions have to be taken into account. Stress-free upper and lower surfaces are considered here, since wave propagation in thin plates are under investigation. Incorporating the corresponding equations one finally ends up with the Rayleigh-Lamb wave equations [7]

$$\frac{\tan(qd)}{\tan(pd)} = \left[-\frac{4k^2pq}{(q^2-k^2)^2} \right]^{(\pm 1)} \tag{2}$$

with p and q being defined as

$$p^2 = \frac{\omega^2}{\sqrt{\frac{\lambda+2\mu}{\rho}}} - k^2 \qquad \text{and} \qquad q^2 = \frac{\omega^2}{\sqrt{\frac{\mu}{\rho}}} - k^2 \quad . \tag{3}$$

Here, ω stands for the circular frequency and k for the circular wavenumber. In the case of an isotropic plate, the main physical effects can be studied on a 2D-model in the plane strain state. This model is also motivated by the accompanying experimental studies. Thus, the multimodal propagating Lamb waves can be divided into symmetric and antisymmetric wave types with respect to the plate centerline, see Fig. 2. The nontrivial solutions of Eq. (2) lead to the dispersion diagram, which is shown for an aluminum plate in Fig. 3. Here, the wavenumbers $\tilde{\nu}$, multiplied by the plate thickness d, of the first symmetric (S_0) and the first antisymmetric (A_0) modes are shown as a function of the product of excitation frequency f and plate thickness d. The dispersive character of the Lamb waves is clearly visible. It

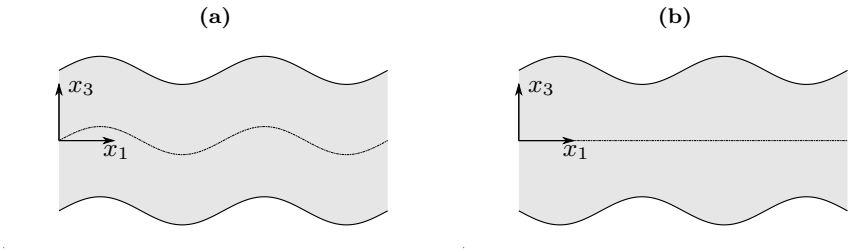

Fig. 2: Sketch of an antisymmetric **(a)** and symmetric **(b)** wave mode in a 2D plate model

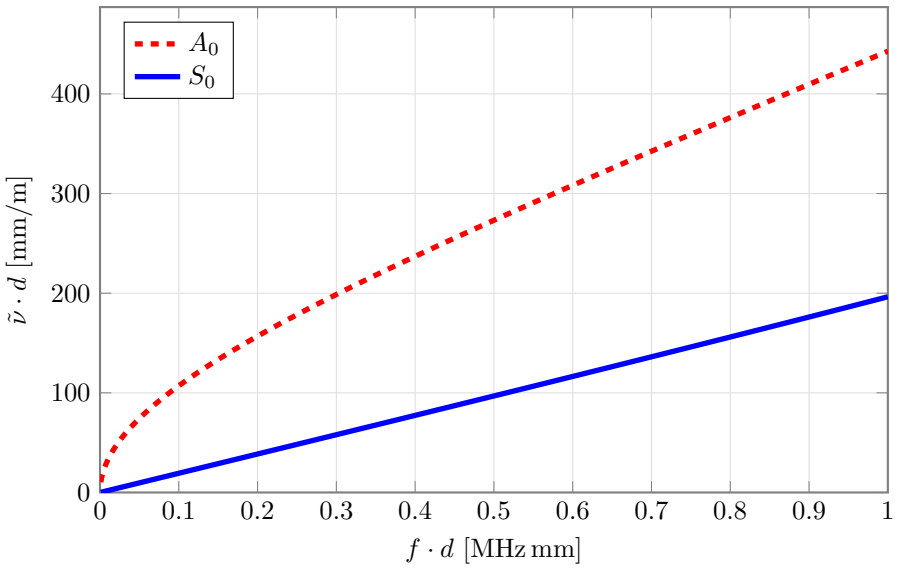

Fig. 3: Analytically computed dispersion diagram for an aluminum plate with the first symmetric (S_0) and the first antisymmetric (A_0) mode

should be noted that higher symmetric and antisymmetric modes are generated at higher frequencies.

With reference to the coordinate system in Fig. 2, the displacements of the symmetric and antisymmetric waves are computed according to [7]

$$\begin{aligned} u_1^{anti} &= \left[ikA_1 \sin(px_3) + qB_2 \sin(qx_3)\right] e^{i(kx_1-\omega t)} \\ u_3^{anti} &= \left[pA_1 \cos(px_3) + ikB_2 \cos(qx_3)\right] e^{i(kx_1-\omega t)} \\ u_1^{sym} &= \left[ikA_2 \cos(px_3) - qB_1 \cos(qx_3)\right] e^{i(kx_1-\omega t)} \\ u_3^{sym} &= \left[-pA_2 \sin(px_3) + ikB_1 \sin(qx_3)\right] e^{i(kx_1-\omega t)} \quad . \end{aligned} \tag{4}$$

The displacement fields show that both the dependence on the coordinate x_1 and the dependence on the time t are represented by a composition of sine and cosine functions. This will be exploited in the application of the Fourier transform in the further course.

2.2 2D Fourier Transform

Multimodal Lamb wave generation already occurs in case of monofrequency excitation, see Fig. 3, and is even more severe with the use of multifrequency excitations, see Sect. 3.2. For this reason, time-based measurement techniques are only suitable to a limited extent for the observation of Lamb waves, since a high effort is necessary to isolate the individual modes. A discrete 2d-FT, on the other hand, is able to select modes even for multimodal and multifrequency measurements, so that the data are analyzed in this way.

Eqs.(4) make it clear that the mathematical description of the symmetric and antisymmetric wave modes is harmonic both in the spatial coordinate x_1 and in time t. To transfer these dependencies in terms of space and time into the frequency

domains, the 2d-FT is used. According to [4], one obtains

$$\mathbf{F}\left(f,\tilde{\nu}\right)=\int_{-\infty}^{\infty}\int_{-\infty}^{\infty}\mathbf{u}(t,x_1)e^{-i2\pi ft}e^{i2\pi\tilde{\nu}x_1}dt\;dx_1 \quad . \tag{5}$$

If one uses 2d-FT for experimental investigation of wave propagation, one captures discrete time signals at predetermined discrete locations, so that Eq. (5) cannot be applied directly. Instead, the 2d discrete Fourier transform is then applied:

$$\mathbf{F}\left(f,\tilde{\nu}\right)=\sum_{x_1=0}^{n}\sum_{t=0}^{m}\left(\mathbf{u}(t,x_1)e^{-i2\pi ft}\right)e^{i2\pi\tilde{\nu}x_1} \quad . \tag{6}$$

From the discrete time signals which is acquired at predetermined spatial points, first the temporal information is transferred into the frequency domain and then the spatial information of the transformed signal is transferred into the wavenumber domain. As a result of this method, a two-dimensional matrix $\mathbf{F}$ with dependencies of the two frequency domains is obtained. This matrix assigns a unique combination of frequency f and wavenumber $\tilde{\nu}$ to each occurring mode and thus enables the separation of the individual modes.

2.3 Accuracy and Measurement Range for 2d-DFT Based Measurements

One of the main concerns of the investigations carried out is to achieve a high degree of accuracy in the measurements. Therefore, based on Eq. (6), the parameters which have an influence on the use of Fourier transforms will be discussed in the following. Likewise, it will be discussed which conditions must be given in order to capture a certain measurement range.

For the accuracy of the measurement, the number of sampled wave periods along the measurement distance is the crucial parameter. In Eq. (6) this influence is reflected by the parameters n and m. It influences the accuracy of the measurement in two ways. On the one hand, it determines the accuracy of the resolution of the FT and on the other hand, the measurement on several wave periods compensates for errors caused by disturbances on individual wave periods. A high number of scannable wave periods requires on the one hand a measurement distance as long as possible, on the other hand a long duration of the measurement. The duration of the measurement is easy to adjust and only affects the size of the resulting data set. The available measurement distance on the specimen, on the other hand, is usually predetermined by the specimen and the measuring system and can therefore only be changed to a limited extent. In Sect.4.2, the influence of these parameters is illustrated using the example of a performed measurement.

The decisive parameter for the possible measurement range is the sampling frequency of the measurement. This parameter is represented in the 2d Fourier transform used here on the one hand by the temporal sampling frequency and on the other hand by the spatial distance of the measuring points. These parameters are only dependent on the measuring system used and the amount of data to be processed and therefore do not place any requirements on the geometry of the specimen.

3 Experimental Procedure

3.1 Specimen and Data Aquisition

For the experimental investigations, an aluminum plate (AlMg3) with dimensions $500 \times 400 \times 2$ mm^3 is used as a specimen, of which the material properties were determined in separate preliminary tests and are given in Table 1. A rectangular piezoelectric wafer with dimensions 5×30 mm^2 and a thickness of 0.2 mm is used to excite the Lamb waves. It is attached to the specimen with epoxy glue and is placed in such a way that the measurements are affected as little as possible by edge reflections, see Figure 4.

The data is acquired using a Polytec PSV-500 laser Doppler vibrometer with a sampling frequency of 3.125 MHz, which results in a maximum detectable signal frequency of 1.5625 MHz, cf. [19]. The excited Lamb waves are then measured on the surface of the specimen along a straight line prepared with a reflective foil, see Fig. 4. This path consists of 430 points with an approximate spacing of 0.66 mm. According to the Nyquist-Shannon sampling theorem [19], this leads to a maximum detectable wavenumber $\tilde{\nu}$ of about 763 m^{-1}. It should be mentioned here that the observation points are not exactly equidistant, which is due to small deviations in the positioning of the laser. A possible influence on the results is compensated by the spatial non-uniformity of the 2d-FT used, see Section 4.5.

As stated in [12, 17], the laser vibrometer measures the velocity component in the direction of the laser beam at specified points on the plate surface. Since the laser beam is essentially perpendicular to the plate surface, the out-of-plane component of the velocity is almost exclusively recorded. This component is significantly larger for the antisymmetric wave than for the symmetric one, so that

Table 1: Specifications of the aluminium specimen

Young's modulus	64.6 GPa
Poisson's ratio	0.33
density	2.7 g/cm^3

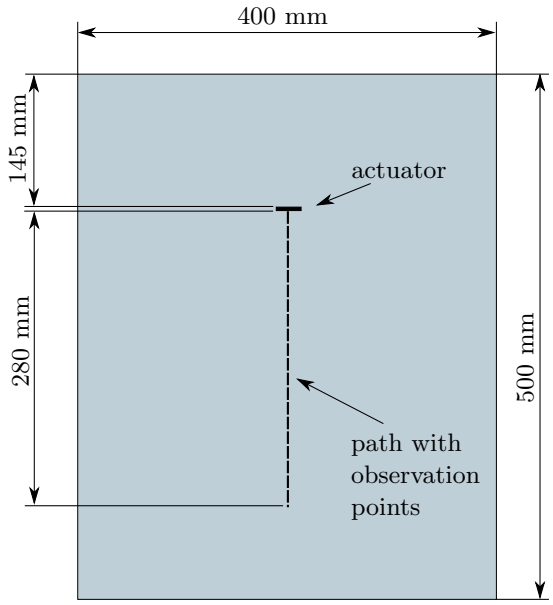

Fig. 4: Sketch of the specimen, the location of the actuator and the path with observation points

the accuracy of the measurements is different for the two modes. This aspect is discussed in Section 4.2 in the context of the experimental investigations.

3.2 Excitation Signal

When selecting an excitation signal, it is advantageous that the 2d-FT does not require special reference points in time or space to evaluate a wave packet. Another advantage is that the 2d-FT is not very sensitive to interference from reflections. So, a multi-frequency excitation signal is used to generate the Lamb waves, see

Fig. 5(a). It consists of superimposed sinusoids with a subsequently applied Hann window, [3].

This signal was chosen from two points of view. First, the signal has a duration of 80 ms and can therefore be considered as long in the context of this application. Thus, as described in Sect 2.3, a high accuracy in the temporal frequency domain is achieved. Second, as shown in the spectrum of the signal in Fig. 5(b) a signal shows clearly separable frequency maxima, which are in 10 kHz distance to one another. This separation is necessary to ensure a high accuracy and reliability of the peak search algorithm, which is used to evaluate the results of the 2d-FT. Table 2 summarizes the data of the excitation signal and additionally shows the data for the spatial and temporal sampling of the measurements.

The excitation signal used here differs significantly from those frequently used in investigations on Lamb waves. These are often very short narrowband sine burst signals or very broadband pulse excitations. The advantage of the signal chosen here is that both a broadband excitation occurs as in pulse excitation, but a good separation of the frequency components is possible. In addition, the accuracy of the temporal frequency in the evaluation is significantly better than with conventionally used excitation signals due to the temporaly long signal.

3.3 2D-FT and Peak Search Algorithm

After measuring the velocities along the measurement path with the laser vibrometer, the data is transferred to the frequency domains using the 2d-FT. The result is a matrix with amplitude values representing the relationship between the two frequency domains. Exemplary this is shown in Fig. 6 in which an evaluation of a

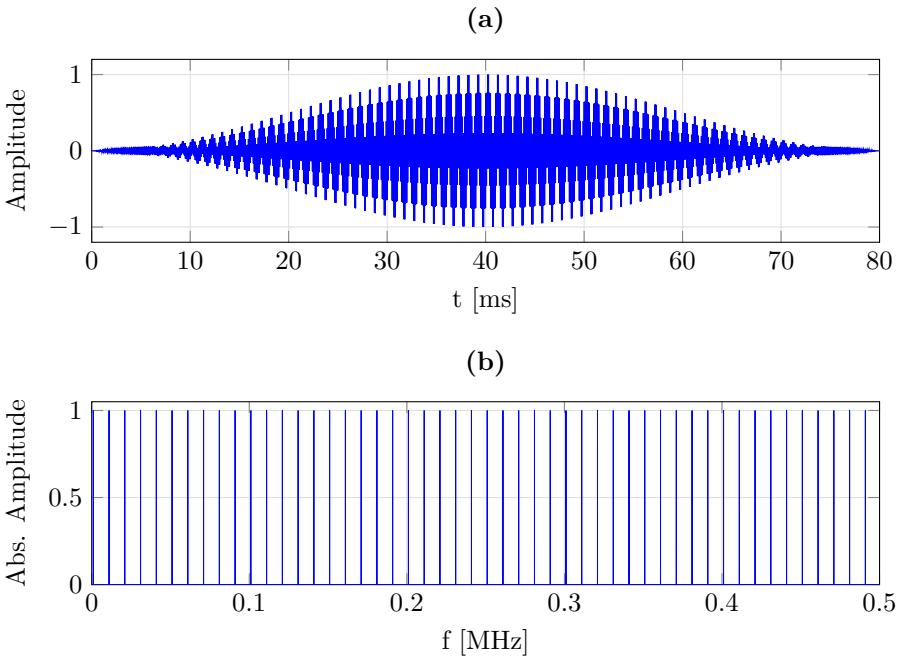

Fig. 5: Excitation signal: **(a)** time domain **(b)** frequency domain

Table 2: Specifications excitation and sampling

Excitation	
spectrum	1:1:500 kHz
excitation time	80 ms
sampling frequency	10 MHz
Spatial Sampling	
measuring length	0.2818 m
number of measurement points	430
distance of measurement points	0.66 mm
maximum detectable wavenumber	763 m^{-1}
Temporal Sampling	
measuring time	80 ms
number of measurement points	250 000
sampling frequency	3.125 MHz
maximum detectable frequency	1.5625 MHz

measurement with an excitation signal including the frequencies from 20 kHz mm to 1 MHz mm in 20 kHz mm steps is shown. It can be seen that clearly recognizable maxima occur at the excited frequencies. Note that for each temporal frequency two significant maxima occur. They represent the first two Lamb waves modes A_0 and S_0 propagating in a straight direction away from the piezoelectric actuator. When considering the maxima, an expected difficulty in the later evaluation becomes clear, namely that the out-of-plane amplitudes of the A_0 wave are significantly larger than those of the S_0 waves. The effects of this difference is discussed in more detail in Sect. 4.2.

In the next step, these maxima are detected automatically with a 2d peak search algorithm and the results of the individual measurements are combined to form the dispersion curves. To save computing time and resources, the evaluation is performed sequentially in several steps so that the accuracy of the results can be increased successively. The first steps take into account the full spectra, but with a low resolution. After the first peak search has been performed, the spectrum is concentrated on these peaks so that the resolution and thus the accuracy can be increased. Splitting the algorithm into several steps has proven worth in execution because it leads to a better use of resources than computing the whole spectra with high resolution in one step.

At this point, it is additionally mentioned that this process only considers waves moving away from the wafer, i.e. only positive wavenumbers are evaluated. The method is also capable of detecting negative wavenumbers but since this is not necessary for the results presented, only positive wavenumbers are included to increase computational efficiency.

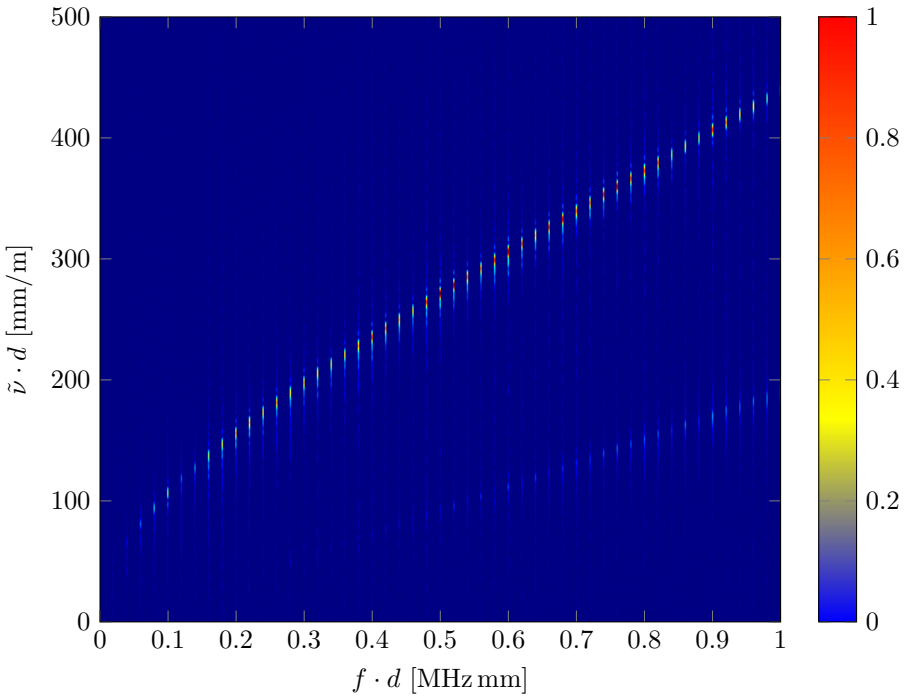

Fig. 6: Dispersion diagram as the 2d-FT solution

4 Results and Discussion

4.1 Experimental Results

Based on the experimental procedure presented in Sect. 3, the dispersive behavior of the guided waves in the aluminum plate is measured and analyzed. To find a solution for a spectrum from 2 kHz mm to 1 MHz mm with steps of 2 kHz mm, ten measurements were performed using the excitation signals specified in Sect. 3.2. The results were evaluated as described in Sect. 3.3. Figure 7 (a) and (c) show the resulting wavenumber frequency relations for the first antisymmetric (A_0) and first symmetric (S_0) mode. In the following, these results are evaluated on the basis of various criteria.

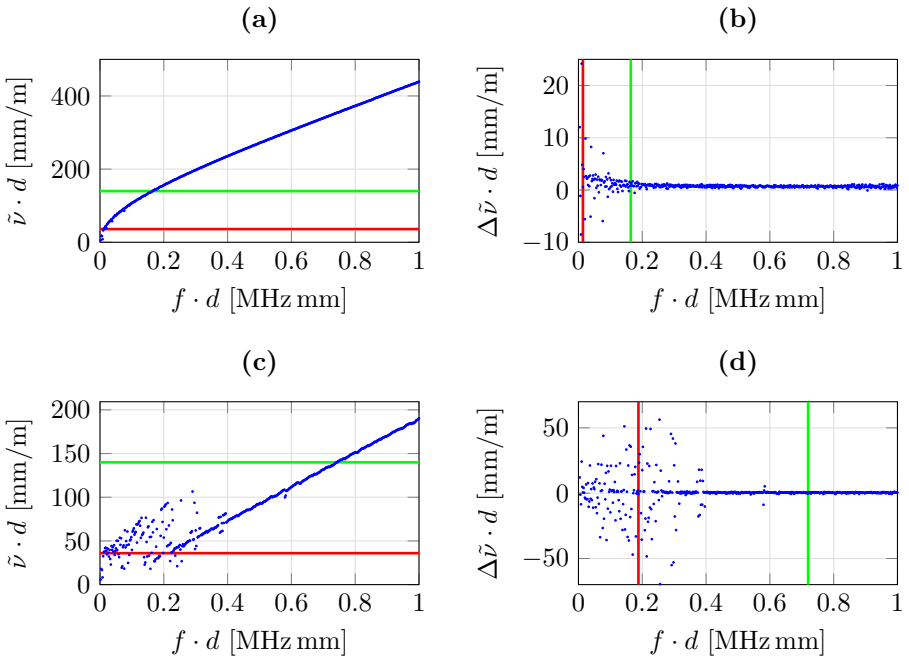

Fig. 7: Experimental data for the aluminium specimen **(a)** and **(c)** dispersion diagrams for A_0 and S_0, **(c)** and **(d)** differences in wavenumber to prior frequency A_0 and S_0

4.2 Evaluability of Experimental Results

As described in Sect. 2.3, there are not only parameters that define the maximum measurable frequency and wavenumber, but there are also quantities that influence the accuracy and evaluability of the measurements. One such quantity is the number of wave periods on the measurement distance. In order to determine an evaluable measurement range, the measurement results are examined for this quantities in the following.

Consideration of the temporal frequency makes it clear that the temporal accuracy is determined only by the duration of the measurement and the excitation signal. Since a long duration excitation signal is used, the accuracy is very high.

Therefore, the peak search algorithm is able to search the data with an accuracy of ± 1 Hz with respect to the expected temporal frequency. As a result, there is almost no loss of accuracy in the results due to frequency deviations.

The accuracy in the wavenumber range, on the other hand, is defined by the length of the measurement distance on the specimen. This length is 0.2818 m and is limited by the specifications of the specimen. Therefore, large inaccuracies are to be expected in the range of small wavenumbers. This is confirmed in Figs. 7 (a) and (c). For small wavenumbers, one can see large scattering in the results of the peak search algorithm. This is particularly observable in the S_0-mode, since for this mode the wavenumber for a larger part of the considered spectrum is significantly smaller than in the antisymmetric mode. As shown in Fig. 7 (b) and (d), this effect can be seen even more clearly if one examines the differences in the wavenumber to the next frequency step in each case. In these diagrams, a clear dependence on the detectable wavenumber can be seen.

Since the length of the specimen determines the measurement distance, it is reasonable to specify a minimum wavenumber for the measurements. This is illustrated by the colored lines along the minimum detectable wavenumbers in Figs. 7 (a) and (c) or frequencies in Fig. 7 (b) and (d).The red line and green line indicate that at least five and twenty sinusoidal sweeps, respectively, were recorded along the measurement distance. In the following observations, the data will be limited to measurements with at least five sinusoidal sweeps in space. This results in a minimum evaluated frequency of 36 kHz mm for A_0 and 188 kHz mm for S_0.

When taking measurements and evaluating the results, it must also be taken into account that the laser vibrometer mainly measures the out-of-plane component of the velocity at the surface. These components are significantly larger for

the A_0 mode than for the S_0 mode. Reflections of the waves occur during the experiments and influence the measurements. The magnitude of these perturbations is significantly larger for the small amplitudes of the S_0 modes than for the larger A_0 modes, therefore the results for this mode are more influenced.

4.3 Reproducability

In the following, the reproducibility of the measurements is considered in more detail. For this purpose, the measurements of the wavenumber frequency pairs, see Sect. 4.1, are repeated and evaluated fifty times. Fig.8 shows the corresponding 95 % confidence intervals and standard deviations as percentages of the respective measured value. In order to be able to present as much data as possible but also make sure that the displayed range is not too strongly influenced by individual outliers, the minimal displayed wavenumber is set to 75 mm/m. This leads to a minimum frequency-thickness value of 48 kHz mm for the A_0 and 388 kHz mm for the S_0 mode. In addition, outliers in the S_0 mode were excluded at frequency-thickness values of 394 kHz mm and 718 kHz mm.

It can be seen that for both the A_0- and the S_0-mode, the values for the standard deviation and the confidence interval are very small and thus the measurements show good reproducibility. Furthermore, it is visible, that the relative measurement inaccuracies decrease with increasing wavenumbers, as expected.

4.4 Comparison to Analytic Solutions

For the evaluation of the quality of the measurement, the measured wavenumber-thickness values are now compared with a linear analytical solution for the prop-

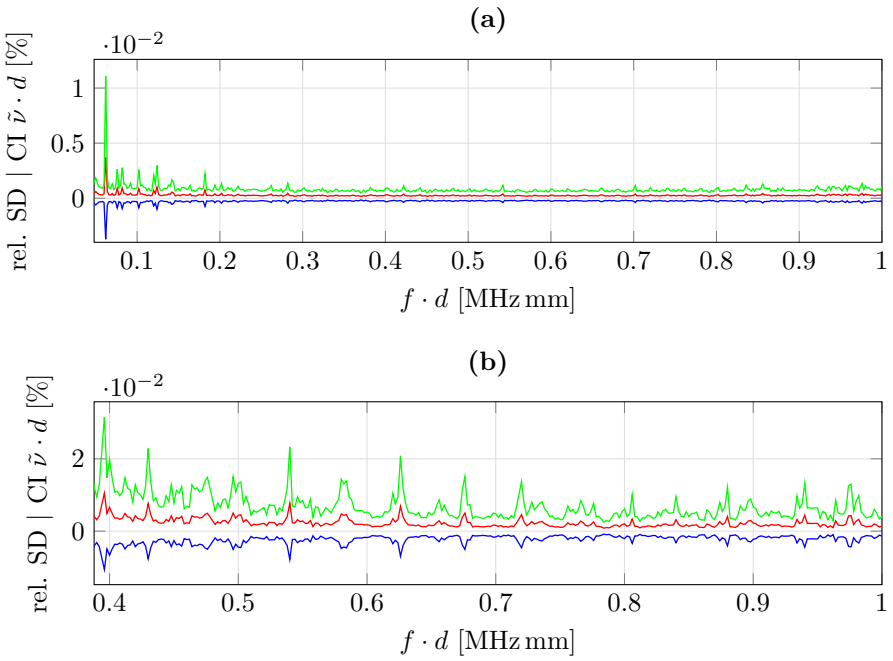

Fig. 8: Relative values for standard deviation (SD, red) and confidence interval (CI, green and blue) based on standard deviation for **(a)** A_0 **(b)** S_0

agation behavior of Lamb waves. Fig. 9 (a) and (c) show the difference between the measurement and the analytical solution for the wavenumber-thickness values as a function of frequency. Fig. 9 (b) and (d) show the relative difference based on the analytical solution. The data show reasonably good accuracy, with the scatter decreasing with increasing frequency respectively wavenumber. The measurement of the antisymmetric mode has high accuracy and shows almost no outliers. Only a larger scatter at low wavenumbers can be seen. The S_0 mode has a significantly higher number of outliers over a larger frequency range. This is due on the one hand to the less steep increase of the wavenumber with frequency and on the other hand to the possible reflections of the A_0 mode. Taking this into account, the measurement is still in very good agreement with the analytical solution.

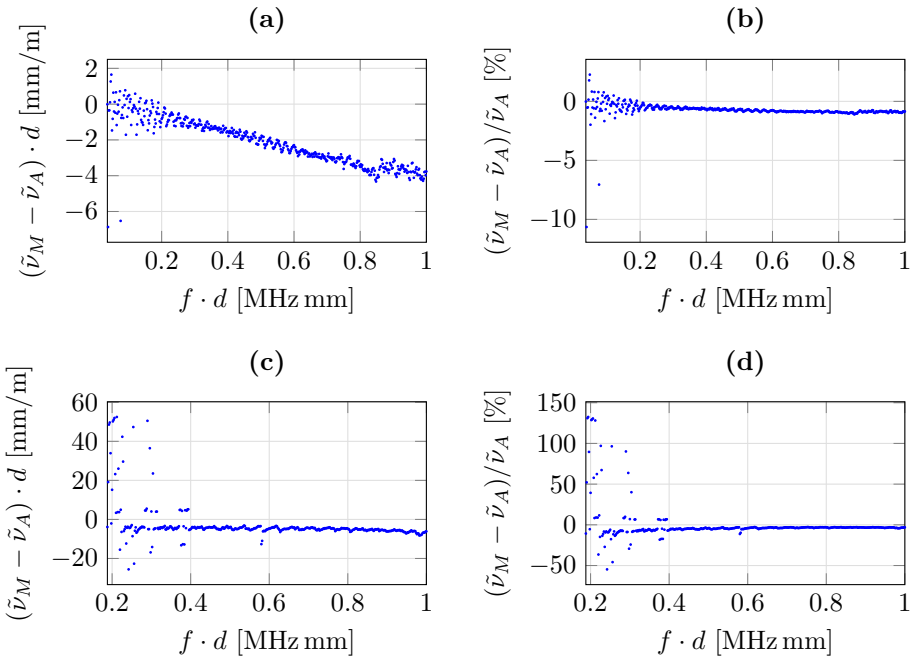

Fig. 9: Differences between experimental and analytic data **(a)** differences in wavenumber-thickness value A_0, **(b)** relative differences in wavenumber-thickness value to analytic values A_0, **(c)** differences in wavenumber-thickness value S_0, **(d)** relative differences in wavenumber-thickness value to analytic value S_0

4.5 Non Uniformity Spacing of Aquisition Points

As already mentioned in Sect. 3.1, the calculation of the 2d-FT uses a method variant which allows non-equidistant measurement points in the spatial domain. This is necessary because the laser cannot be positioned on exactly equidistant observation points. In the following, the errors, which result from the assumption of uniformly distributed measuring points resp. a uniform DFT, are considered in more detail. For comparison, an equal distance between the individual measurement points is assumed, i.e., the start and end points of the measurement distance are used and the distance is divided equally over the number of measurement points. The data were obtained in the frequency ranges defined in Sect. 4.2.

Furthermore, outliers were excluded from the analysis as they do not provide any information about the difference between the results of the different measurement point distributions.

Fig. 10 (a) shows the difference in the location of the measurement points over the measurement distance compared to equidistant spacing. Fig. 10 (b), on the other hand, depicts the difference in spacing between successive measurement points. The measurement data are now re-evaluated assuming an equal distribution of measurement points and compared with the results of the non-equodistant solution. Thus, the errors resulting from not considering the uneven distribution can be analyzed. Fig. 10 (c) represents the difference in wavenumbers over the detected wavenumbers. It can be seen that not taking into account the non-uniform spacing leads to an error in the evaluation. As expected, this error depends on the wavenumber to be evaluated.

In order to be able to make a statement about the improvement of the measuring accuracy, Fig. 10 (d) shows the relative wavenumbers with respect to the data of the analytical solution for both modes and for the equidistant (index U) as well as the non-equidistant (index NU) evaluations. It becomes visible that the use of the 2d-FT for non-equidistant measurement points increases the accuracy for both modes. The obtained improvement of the data is in the range of 0.5 %. Comparing this value with the deviations of the measurement to the analytical solutions shows that the deviations from the analytical solution are also in the low single-digit percentage range. Thus it can be stated that the use of the non-uniform FT for the spatial domain represents a significant improvement of the measuring method.

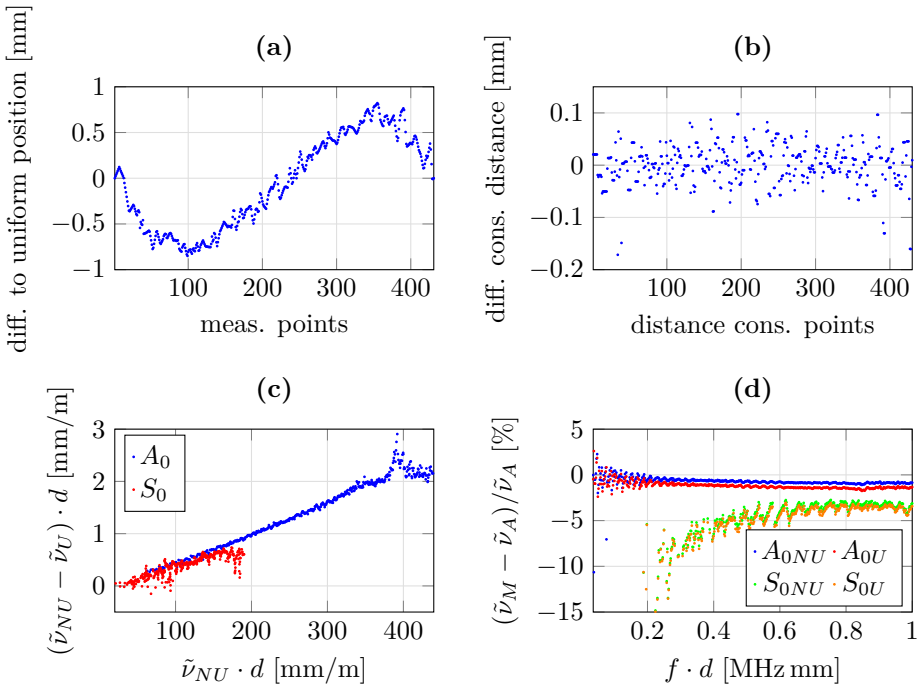

Fig. 10: **(a)** differences between non-equidistant and equidistant location of the measurement points, **(b)** spacing between consecutive measurement points, **(c)** differences in wavenumber between non-equidistant and equidistant data, **(d)** relative differences in wavenumber between measurements and analytic results for non-equidistant (NU) and equidistant (U) data.

Considering that the distances of the measuring points do not show large differences in the measurements performed, this effect can become especially important for those measurements where there is a more non-uniform spacing of the measuring points due to the measuring system or the specification of the specimen.

5 Conclusion

In this work, the potential offered by the 2d Fourier transform as a tool for measuring the dispersive properties of Lamb waves is demonstrated. It is worked out

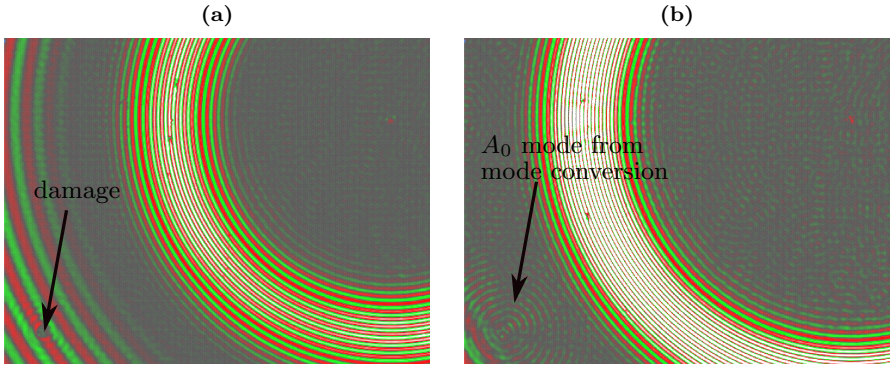

Fig. 11: Interaction of symmetric Lamb waves with artificial damage (lower left) at two time points.

that the proposed method can be used to measure the velocity of Lamb waves in a time-saving manner, especially when the velocities of different wave modes in a frequency range need to be determined. In comparison to an analytical solution, it was also shown that a high measurement accuracy is achieved.

Since Lamb waves are of particular importance in the field of structural health monitoring, the present investigations must be extended to study the influence of damage or edges on the measurement method. This need is illustrated by Fig. 11, which shows the behavior of symmetric Lamb waves in the presence of artificial damage caused by an additional mass. The symmetric Lamb waves pass through the damage site and cause both reflections and interactions, which are shown at an early time on the left and at a later time on the right. The effects of these reflections and interactions on the accuracy of the measurements will be investigated in later work. In addition, specimens made of aluminum or fiber-metal laminates that are under prestress or contain residual stresses will also be studied using the presented method.

Declarations

Conflicts of interests: The authors have no conflicts of interest to declare that are relevant to the content of this article.

Financial/non-financial interests: All authors certify that they have no affiliations with or involvement in any organization or entity with any financial interest or non-financial interest in the subject matter or materials discussed in this manuscript. Also the authors have no financial or proprietary interests in any material discussed in this article.

Funding: No funding was received for conducting this study.

References

1. Achenbach, J.D.: Wave propagation in elastic solids, by J. D. Achenbach. North-Holland Pub. Co.; American Elsevier Pub. Co Amsterdam, New York (1973)
2. Alleyne, D., Cawley, P.: A two-dimensional fourier transform method for the measurement of propagating multimode signals. The Journal of the Acoustical Society of America **89**(3), 1159–1168 (1991). DOI 10.1121/1.400530
3. Blackman, R., Tukey, J.: The Measurement of Power Spectra, from the Point of View of Communications Engineering. Dover Publications (1959)
4. Bracewell, R.N., Bracewell, R.N.: The Fourier transform and its applications, vol. 31999. McGraw-Hill New York (1986)
5. Gao, F., Zeng, L., Lin, J., Zhi, L.: Mode separation in frequency-wavenumber domain through compressed sensing of far-field lamb waves. Measurement Science and Technology **28** (2017). DOI 10.1088/1361-6501/aa6c54
6. Giurgiutiu, V.: Structural Health Monitoring. Academic Press, Burlington (2008). DOI 10.1016/B978-0-12-088760-6.50020-9
7. Graff, K.: Wave Motion in Elastic Solids. Dover Books on Physics. Dover Publications (2012)
8. Grondel, S., Assaad, J., Delebarre, C., Blanquet, P., Moulin, E.: The propagation of lamb waves in multilayered plates: Phase-velocity measurement. Measurement Science and Technology **10**, 348–353 (1999). DOI 10.1088/0957-0233/10/5/002
9. Hora, P., Červená, O.: Determination of lamb wave dispersion curves by means of fourier transform. Appl. Comput. Mech. **6**, 5–16 (2012)
10. Lamb, H.: On waves in an elastic plate. Proceedings of the Royal Society of London. Series A, Containing Papers of a Mathematical and Physical Character **93**(648), 114–128 (1917)
11. Lammering, R., Gabbert, U., Sinapius, M., Schuster, T., Wierach, P.: Lamb-Wave Based Structural Health Monitoring in Polymer Composites. Springer International Publishing (2018). DOI 10.1007/978-3-319-49715-0
12. Neumann, M., Hennings, B., Lammering, R.: Identification and avoidance of systematic measurement errors in lamb wave observation with one-dimensional scanning laser vibrometry. strain **49**(2), 95–101 (2013). DOI 10.1111/str.12015

13. Neumann, M.N., Hennings, B., Lammering, R.: Quasi-Continuous Mode Conversion of Lamb Waves in CFRP Plates Due to Inhomogeneity on Micro and Meso Scale. In: L. Cam, Vincent, Mevel, Laurent, Schoefs, Franck (eds.) EWSHM - 7th European Workshop on Structural Health Monitoring. IFFSTTAR, Inria, Université de Nantes, Nantes, France (2014)
14. Niethammer, M., Jacobs, L., Qu, J., Jarzynski, J.: Time-frequency representation of lamb waves. The Journal of the Acoustical Society of America **109**, 1841–7 (2001). DOI 10.1121/1.1357813
15. Prosser, W., Seale, M., Smith, B.: Time-frequency analysis of the dispersion of lamb modes. The Journal of the Acoustical Society of America **105**(5), 2669—2676 (1999). DOI 10.1121/1.426883
16. Rose, J.L.: Ultrasonic Guided Waves in Solid Media. Cambridge University Press (2014). DOI 10.1017/CBO9781107273610
17. Schell, J., Behrend, R., Neumann, M., Lammering, R.: Structural health monitoring using lamb wave testing structural health monitoring using lamb wave testing identifying defects per scanning laser vibrometry application note. Polytec GmbH (2017)
18. Schöpfer, F., Binder, F., Woestehoff, A., Schuster, T., V. Ende, S., Föll, S., Lammering, R.: Accurate determination of dispersion curves of guided waves in plates by applying the matrix pencil method to laser vibrometer measurement data. CEAS Aeronautical Journal **4**, 61–68 (2013)
19. Shannon, C.: Communication in the presence of noise. Proceedings of the IRE **37**(1), 10–21 (1949). DOI 10.1109/jrproc.1949.232969
20. Staszewski, W.J., Lee, B.C., Mallet, L., Scarpa, F.: Structural health monitoring using scanning laser vibrometry: I. lamb wave sensing. Smart Materials and Structures **13**(2), 251–260 (2004). DOI 10.1088/0964-1726/13/2/002
21. Su, Z., Ye, L.: Identification of Damage Using Lamb Waves: From Fundamentals to Applications, vol. 48. Springer, London (2009). DOI 10.1007/978-1-84882-784-4
22. Viktorov, I.A.: Rayleigh and lamb waves: Physical theory and applications. Plenum Press, New York (1967)
23. Wilcox, P., Lowe, M., Cawley, P.: The effect of dispersion on long-range inspection using ultrasonic guided waves. NDT & E International **34**(1), 1–9 (2001). DOI 10.1016/S0963-

8695(00)00024-4